

Periodic table for highly charged ions

Chunhai Lyu,* Christoph H. Keitel, and Zoltán Harman
Max-Planck-Institut für Kernphysik, Saupfercheckweg 1, 69117 Heidelberg, Germany
(Dated: April 16, 2025)

Mendeleev’s periodic table successfully groups atomic elements according to their chemical and spectroscopic properties. However, it becomes less sufficient in describing the electronic properties of highly charged ions (HCIs) in which many of the outermost electrons are ionized. In this work, we put forward a periodic table particularly suitable for HCIs. It is constructed purely based on the successive electron occupation of relativistic orbitals. While providing a much-simplified description of the level structure of highly charged isoelectronic ions – essential for laboratory and astrophysical plasma spectroscopies, such a periodic table predicts a large family of highly forbidden transitions suitable for the development of next-generation optical atomic clocks. Furthermore, we also identify universal linear Z scaling laws (Z is the nuclear charge) in the so-called “Coulomb splittings” between angular momentum multiplets along isoelectronic sequences, complementing the physics of electron-electron interactions in multielectron atomic systems.

Introduction — In multielectron atomic physics, the ‘building-up’ principle [1] states that the electron would fill atomic orbitals according to their relative energies. For neutral atoms, the repulsion interaction between electrons renders the $(n+1)s$, $(n+1)p$ orbitals asserting energies lower than those of the nd , nf orbitals, with n being the principal quantum number, and s, p, d, f corresponding to orbital angular momenta $l = 0, 1, 2, 3$, respectively. As a consequence, the electron would fill atomic orbitals according to the increasing value of $n+l$. This principle, also called Madelung–Janet rule [1], determines the ground-state electron configurations, thus the physical and chemical properties of the corresponding transition metal, lanthanoid and actinoid elements in the conventional periodic table [2].

However, when the outer-shell electrons of an atom are stripped off, it becomes a highly charged ion (HCI). Though such systems are exotic, they play a key role in laboratory and astrophysical plasmas [3–5], x-ray lasers [6–8], nanolithography [9], tumor therapy [10], optical clocks [11–13], and in testing fundamental theories [14–16]. As the electrons in HCIs feel a much stronger Coulomb interaction with the nucleus, the electrons would follow the so-called Coulomb filling rule [17]: i.e., before occupying the $(n+1)$ -th shell, the electron will first fill out all the orbitals in the n -th shell.

Periodic table — Here, we show that the Coulomb filling rule renders it possible to construct a meaningful new periodic table for HCIs. This allows us to gain extraordinary insight into the physics and applications of such strong-field multielectron systems. As shown in Fig. 1, in the newly proposed periodic table, each cell represents an isoelectronic sequence, containing tens of ions sharing the same relativistic valence-electron configuration nl_{\pm}^m (m is the number of electrons in the corresponding relativistic orbital, and the subscripts \pm stand for the single-electron total angular momentum $j = l \pm 1/2$, respectively). Then,

each column groups cells with the same j^m multiplet, and each row (period) collects cells with the same nl_{\pm} values, where ns , np_{-} and np_{+} orbitals are put in the same row to save space. As both np_{+} and nd_{-} have $j = 3/2$, and both nd_{+} and nf_{-} have $j = 5/2$, they are grouped into the same column, respectively.

Different from the conventional periodic table where nl_{-} and nl_{+} orbitals are treated equivalently due to strong LS couplings, in our case for HCIs with strong jj couplings, the electrons will first fill the nl_{-} orbital. Only after nl_{-} is fully occupied with $2j+1$ electrons, the remaining electron can start to fill the nl_{+} orbital. Such an arrangement is straightforward as Dirac’s relativistic theory [18, 19] predicts a lower orbital energy for nl_{-} than that for its nl_{+} counterpart. However, to have the abovementioned filling order, the fine-structure splittings between nl_{-} and nl_{+} shall exceed the energy caused by electron-electron interactions. The ion at the bottom of each cell benchmarks the lightest element at which this rule is fulfilled, thus resembles the crossing point from LS couplings to jj couplings.

This new periodic table would bear significant consequences for the understanding and applications of HCIs in fields ranging from atomic physics and quantum optics, to plasma spectroscopy and astrophysics, and to ultraprecise clocks.

Ground states — As a first consequence, the periodic table in Fig. 1 enormously simplifies the spectroscopic analysis of complex atomic structures. It is well known that atomic systems with partially filled d and f orbitals contain tremendously complicated fine-structure terms [18, 21]. Without numerical calculations, it is difficult to identify their ground states [22]. However, our new periodic table introduces additional closed-shell configurations, namely, the columns with fully occupied np_{-}^2 , nd_{\pm}^1 , and nf^0 configurations. Based on this, it allows one to define new valence electron configurations and their corresponding hole states. Therefore, the ground state of HCIs can be easily identified by analyzing the angular couplings of these simplified electron configurations. The results are shown at the bottom of the periodic table

* chunhai.lyu@mpi-hd.mpg.de

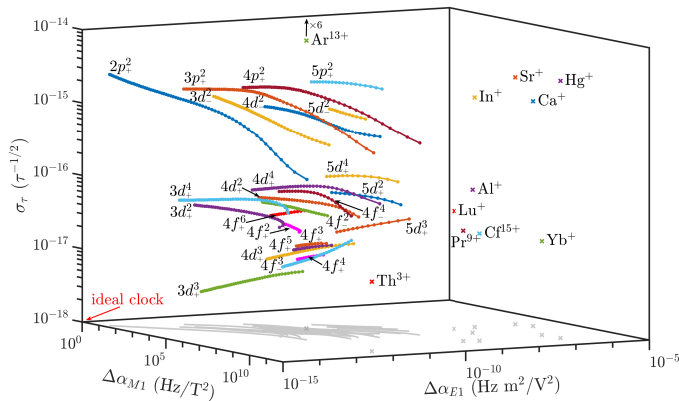


Figure 3. **Superior clock properties of HCI clock candidates.** The projected instability σ_τ , differential magnetic ($\Delta\alpha_{M1}$) and electric-dipole ($\Delta\alpha_{E1}$) polarizability of over 700 HCI clock candidates are plotted, with the grey lines and crosses being their projections in the $x-y$ plane. Each line corresponds to a relevant isoelectronic sequence denoted by the colored cells in the periodic table Fig. 1. The values for state-of-the-art singly charged ion clocks [12, 42], Ar^{13+} [11], Pr^{9+} [43], Cf^{15+} [44], and nuclear clock $^{229}\text{Th}^{3+}$ [45] are presented for comparison.

constructed and planned clock references [12, 13], as depicted by the crosses in Fig. 3, these HCI clock references are far less sensitive to perturbations of external electromagnetic fields. Therefore, they would result in black-body radiation shifts, AC Stark shifts and second-order Zeeman shifts, all up to 3 to 5 orders of magnitude smaller than those of state-of-the-art clocks [46, 47], as well as the planned $^{229}\text{Th}^{3+}$ nuclear clock [48], rendering it possible to demonstrate clocks with fractional precision $\delta\nu/\nu < 10^{-20}$. High-precision spectroscopy [49] of the isotope shifts of this vast range of narrow transitions would find applications in, e.g., King-plot analysis [50–52], and thus enriching the test of nuclear theories and the search for physics beyond the standard model [53].

Coulomb splitting — The emergence of the physics discovered above can be illustrated in Fig. 4. Here, the evolution of the energies of the low-lying states, as a function of nuclear charge Z , are plotted for isoelectronic systems of nd^2 , nd_+^2 , nd_+^3 , and nd_+^4 ($n = 3, 4, 5$) configurations. While these states intertwined together in the cases of light elements (i.e., small Z), it is obvious that their excitation energies evolve into two distinct scaling laws for heavy ions (i.e., large Z). For states involving electron excitations between the l_- and l_+ orbitals, their energies scale as Z^4/n^3 that feature the Z^2Z^{*2}/n^3 scaling laws for the relativistic fine-structure splittings [18, 54] (Z^* is the effective charge under electron screening effect).

For states whose energies scale linearly with Z in Fig. 4,

they are all from the corresponding ground-state configurations listed in the bottom row of the periodic table (Fig. 1). In the case of nd_+^2 , our analytical calculation predicts

$$E_2 - E_4 = \frac{24}{175}R_2 - \frac{2}{63}R_4, \quad (1)$$

$$E_0 - E_4 = \frac{12}{35}R_2 + \frac{1}{9}R_4. \quad (2)$$

Here, $E_{0,2,4}$ are the energies of the $J = 0, 2, 4$ states, respectively, with $R_k = \int dr_1 \int dr_2 \rho(r_1)\rho(r_2)r_{<}^k/r_{>}^{k+1}$ [$k = 2, 4$, and $r_{>} = \max(r_1, r_2)$ and $r_{<} = \min(r_1, r_2)$] being the Slater integral of rank k [18, 54], and $\rho(r)$ the electron density of the radial wavefunction of the nd_+ orbital. As $R_k \propto \langle \frac{1}{r} \rangle \propto Z/n^2$ [18] is a measure of the electron-electron interactions, Eqs. (1,2) indicate that there is a significant cross cancellation of relativistic effects in the energy splittings between these states. Due to such a linear scaling law, as shown in Fig. 4, the energies of these states quickly become well isolated from those of the states involving inter-orbital excitations. As a consequence, it leads to the reordering of the fine-structure terms, and to the highly forbidden optical and XUV transitions discussed in Fig. 3. The slopes of the lines would thus directly reflect the strengths of the electron-electron interactions in these ions. In the periodic table of Fig. 1, the reference ions at which the first term reordering happens are displayed at the bottom of each cell. This mechanism also explains the grouped level structures of the excited $3d_+^{l-}q3d_+^q$ configurations observed in Fig 2.

In conclusion, our newly introduced periodic table facilitates the spectroscopic analysis of the grouped level structures in complex highly charged atomic systems, which might find applications in various plasma researches. With a single, simple theory under angular momentum couplings of relativistic orbitals, we are able to discover and categorize hundreds of ultrastable HCI clock candidates, whose projected performance could surpass state-of-the-art clocks by several orders of magnitude. Furthermore, with both numerical and analytical methods, we also identify the universal Z/n^2 scaling laws in the energy splittings between states from the same relativistic configurations in HCIs. As these splittings are a consequence of the electron-electron interaction terms in the multielectron atomic Hamiltonian [18, 54], the observed linear scaling laws complement the quadratic Z^2/n^2 scaling laws in principal energies governed by the central Coulomb potential of the nucleus, and the Z^4/n^3 scaling laws in fine-structure splittings manifested by the relativistic effects. To distinguish it from the well-known fine-structure splitting, we suggest to name this type of splitting “Coulomb splitting”. These Z scaling laws would provide a systematic understanding of the spectroscopic properties of HCIs in various plasma conditions.

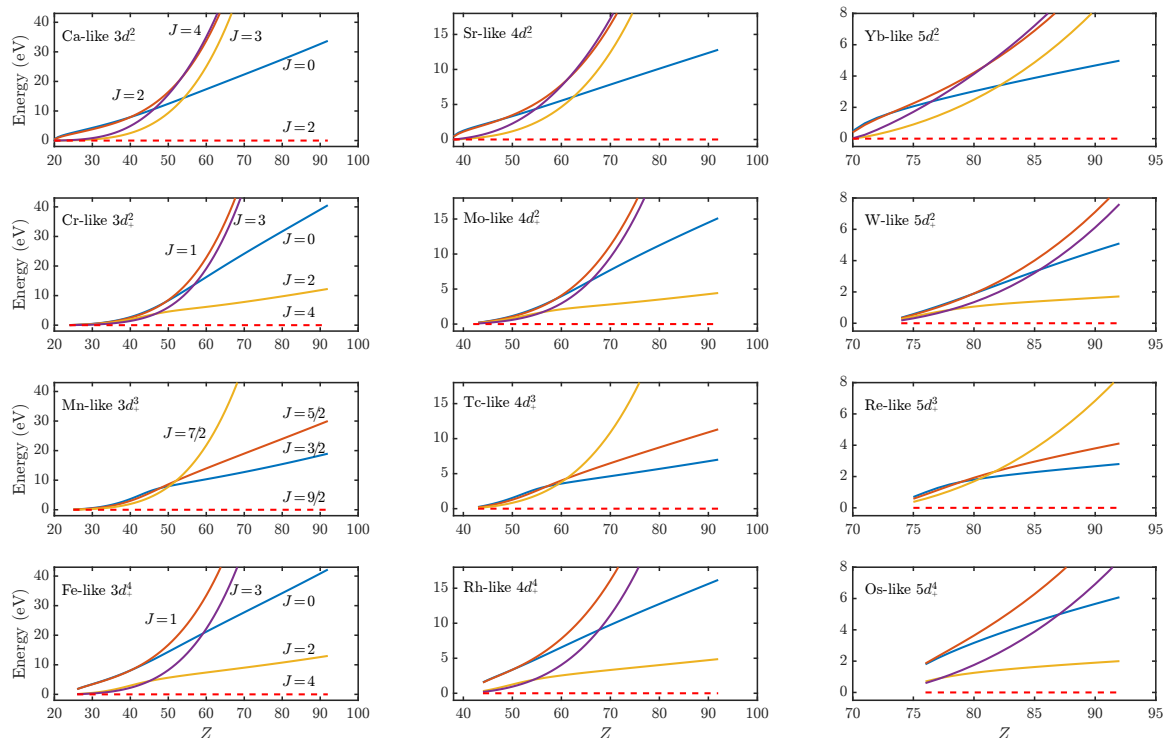


Figure 4. **Universal linear scaling laws manifested by mutual-electron interactions.** Energies of the low lying levels of the nd_{-}^2 , nd_{+}^2 , nd_{+}^3 , and nd_{+}^4 ions are plotted as functions of the atomic number Z . The energies scale linearly with Z are all from the ground-state multiplets listed at the bottom of the periodic table in Fig. 1.

-
- [1] C. J. Foot, *Atomic Physics*, Vol. 7 (Oxford University Press, 2005).
- [2] P. Schwerdtfeger, O. R. Smits, and P. Pyykkö, The periodic table and the physics that drives it, *Nat. Rev. Chem.* **4**, 359 (2020).
- [3] P. Beiersdorfer, K. Boyce, G. Brown, H. Chen, S. Kahn, R. Kelley, M. May, R. Olson, F. Porter, C. Stahle, *et al.*, Laboratory simulation of charge exchange-produced x-ray emission from comets, *Science* **300**, 1558 (2003).
- [4] S. Bernitt, G. V. Brown, J. K. Rudolph, R. Steinbrügge, A. Graf, M. Leutenegger, S. W. Epp, S. Eberle, K. Kubiček, V. Mäckel, *et al.*, An unexpectedly low oscillator strength as the origin of the Fe XVII emission problem, *Nature* **492**, 225 (2012).
- [5] L. Schmöger, O. Versolato, M. Schwarz, M. Kohnen, A. Windberger, B. Piest, S. Feuchtenbeiner, J. Pedregosa-Gutierrez, T. Leopold, P. Micke, *et al.*, Coulomb crystallization of highly charged ions, *Science* **347**, 1233 (2015).
- [6] J. Zhang, A. MacPhee, J. Lin, E. Wolfrum, R. Smith, C. Danson, M. Key, C. Lewis, D. Neely, J. Nilsen, *et al.*, A saturated x-ray laser beam at 7 nanometers, *Science* **276**, 1097 (1997).
- [7] A. Depresseux, E. Oliva, J. Gautier, F. Tissandier, J. Nejdl, M. Kozlova, G. Maynard, J. Goddet, A. Tafzi, A. Lifshitz, *et al.*, Table-top femtosecond soft-X-ray laser by collisional ionization gating, *Nature Photonics* **9**, 817 (2015).
- [8] C. Lyu, S. M. Cavaletto, C. H. Keitel, and Z. Harman, Narrow-band hard-x-ray lasing with highly charged ions, *Sci. Rep.* **10**, 9439 (2020).
- [9] J. Sheil, L. Poirier, A. C. Lassise, D. J. Hemminga, S. Schouwenars, N. Braaksma, A. Frenzel, R. Hoekstra, and O. O. Versolato, Power-law scaling relating the average charge state and kinetic energy in expanding laser-driven plasmas, *Phys. Rev. Lett.* **133**, 125101 (2024).
- [10] D. Schardt, T. Elsässer, and D. Schulz-Ertner, Heavy-ion tumor therapy: physical and radiobiological benefits, *Rev. Mod. Phys.* **82**, 383 (2010).
- [11] S. A. King, L. J. Spieß, P. Micke, A. Wilzewski, T. Leopold, E. Benkler, R. Lange, N. Huntemann, A. Surzhykov, V. A. Yerokhin, *et al.*, An optical atomic clock based on a highly charged ion, *Nature* **611**, 43 (2022).
- [12] A. D. Ludlow, M. M. Boyd, J. Ye, E. Peik, and P. O. Schmidt, Optical atomic clocks, *Rev. Mod. Phys.* **87**, 637 (2015).
- [13] M. G. Kozlov, M. S. Safronova, J. R. Crespo López-Urrutia, and P. O. Schmidt, Highly charged ions: Optical clocks and applications in fundamental physics, *Rev. Mod. Phys.* **90**, 045005 (2018).
- [14] J. Morgner, B. Tu, C. König, T. Sailer, F. Heiße, H. Bekker, B. Sikora, C. Lyu, V. Yerokhin, Z. Harman, *et al.*, Stringent test of QED with hydrogen-like tin, *Nature* **622**, 53 (2023).
- [15] R. Loetzsch, H. F. Beyer, L. Duval, U. Spillmann,

- D. Banaś, P. Dergham, F. Kröger, J. Glorius, R. E. Grisenti, M. Guerra, *et al.*, Testing quantum electrodynamics in extreme fields using helium-like uranium, *Nature* **625**, 673 (2024).
- [16] J. C. Berengut, V. A. Dzuba, and V. V. Flambaum, Enhanced laboratory sensitivity to variation of the fine-structure constant using highly charged ions, *Phys. Rev. Lett.* **105**, 120801 (2010).
- [17] S. Goudsmit and P. I. Richards, The order of electron shells in ionized atoms, *Proc. Natl. Acad. Sci.* **51**, 664 (1964).
- [18] I. P. Grant, *Relativistic quantum theory of atoms and molecules: theory and computation* (Springer, 2007).
- [19] P. A. M. Dirac, *The principles of quantum mechanics*, 27 (Oxford university press, 1981).
- [20] H. Gomes, pgf-PeriodicTable – Create custom periodic tables of elements (ver. 2.1.1), [Online]. Available: <https://ctan.org/pkg/pgf-periodictable?lang=en> [2024, July 7th]. (2024).
- [21] P. W. Atkins, J. De Paula, and J. Keeler, *Physical Chemistry* (Oxford University Press, 2023).
- [22] G. C. Rodrigues, P. Indelicato, J. P. Santos, P. Patté, and F. Parente, Systematic calculation of total atomic energies of ground state configurations, *At. Data Nucl. Data Tables* **86**, 117 (2004).
- [23] C. Froese-Fischer, G. Gaigalas, P. Jönsson, and J. Bieroń, GRASP2018—a Fortran 95 version of the general relativistic atomic structure package, *Computer Physics Communications* **237**, 184 (2019).
- [24] H. K. Chung, M. H. Chen, W. L. Morgan, Y. Ralchenko, and R. W. Lee, Flychk: Generalized population kinetics and spectral model for rapid spectroscopic analysis for all elements, *High Energy Density Phys.* **1**, 3 (2005).
- [25] F. B. Rosmej, V. A. Astapenko, and V. S. Lisitsa, *Plasma atomic physics*, Vol. 650 (Springer, 2021).
- [26] J. S. Kaastra, A. J. J. Raassen, J. de Plaa, and L. Gu, SPEX X-ray spectral fitting package (2024).
- [27] L. Mercadier, A. Benediktovitch, Š. Krušič, J. J. Kas, J. Schlappa, M. Agåker, R. Carley, G. Fazio, N. Gerasimova, Y. Y. Kim, *et al.*, Transient absorption of warm dense matter created by an x-ray free-electron laser, *Nature Physics* **20**, 1564 (2024).
- [28] T. Pütterich, R. Neu, R. Dux, A. Whiteford, M. O’Mullane, t. ASDEX Upgrade Team, *et al.*, Modelling of measured tungsten spectra from ASDEX upgrade and predictions for ITER, *Plasma Phys. Control. Fusion* **50**, 085016 (2008).
- [29] A. Kramida and T. Shirai, Energy levels and spectral lines of tungsten, W III through W LXXIV, *At. Data Nucl. Data Tables* **95**, 305 (2009).
- [30] P. Beiersdorfer, Highly charged ions in magnetic fusion plasmas: research opportunities and diagnostic necessities, *J. Phys. B* **48**, 144017 (2015).
- [31] M. O. Scully and M. S. Zubairy, *Quantum optics* (Cambridge university press, 1997).
- [32] C. Brif, R. Chakrabarti, and H. Rabitz, Control of quantum phenomena: past, present and future, *New J. Phys.* **12**, 075008 (2010).
- [33] B. W. Adams, C. Buth, S. M. Cavaletto, J. Evers, Z. Harman, C. H. Keitel, A. Pálffy, A. Picón, R. Röhlsberger, Y. Rostovtsev, *et al.*, X-ray quantum optics, *J. Mod. Opt.* **60**, 2 (2013).
- [34] K. P. Heeg, A. Kaldun, C. Strohm, C. Ott, R. Subramanian, D. Lentrodt, J. Haber, H.-C. Wille, S. Goerttler, R. Ruffer, *et al.*, Coherent x-ray–optical control of nuclear excitons, *Nature* **590**, 401 (2021).
- [35] K. P. Heeg, A. Kaldun, C. Strohm, P. Reiser, C. Ott, R. Subramanian, D. Lentrodt, J. Haber, H.-C. Wille, S. Goerttler, *et al.*, Spectral narrowing of x-ray pulses for precision spectroscopy with nuclear resonances, *Science* **357**, 375 (2017).
- [36] J. Haber, X. Kong, C. Strohm, S. Willing, J. Gollwitzer, L. Bocklage, R. Ruffer, A. Pálffy, and R. Röhlsberger, Rabi oscillations of x-ray radiation between two nuclear ensembles, *Nat. Photonics* **11**, 720 (2017).
- [37] S. M. Cavaletto, Z. Harman, C. Ott, C. Buth, T. Pfeifer, and C. H. Keitel, Broadband high-resolution x-ray frequency combs, *Nat. Photonics* **8**, 520 (2014).
- [38] C. Lyu, S. M. Cavaletto, C. H. Keitel, and Z. Harman, Interrogating the temporal coherence of euv frequency combs with highly charged ions, *Phys. Rev. Lett.* **125**, 093201 (2020).
- [39] A. Derevianko, V. A. Dzuba, and V. V. Flambaum, Highly charged ions as a basis of optical atomic clockwork of exceptional accuracy, *Phys. Rev. Lett.* **109**, 180801 (2012).
- [40] C. Lyu, C. H. Keitel, and Z. Harman, Ultrastable and ultra-accurate clock transitions in open-shell highly charged ions, *Communications Physics* **8**, 3 (2025).
- [41] K. Kromer, C. Lyu, M. Door, P. Filianin, Z. Harman, J. Herkenhoff, P. Indelicato, C. H. Keitel, D. Lange, Y. N. Novikov, C. Schweiger, S. Eliseev, and K. Blaum, Observation of a low-lying metastable electronic state in highly charged lead by penning-trap mass spectrometry, *Phys. Rev. Lett.* **131**, 223002 (2023).
- [42] K. J. Arnold, R. Kaewuam, A. Roy, T. R. Tan, and M. D. Barrett, Blackbody radiation shift assessment for a lutetium ion clock, *Nat. Commun.* **9**, 1 (2018).
- [43] H. Bekker, A. Borschevsky, Z. Harman, C. H. Keitel, T. Pfeifer, P. O. Schmidt, J. R. Crespo López-Urrutia, and J. C. Berengut, Detection of the $5p-4f$ orbital crossing and its optical clock transition in Pr^{9+} , *Nat. Commun.* **10**, 1 (2019).
- [44] J. C. Berengut, V. A. Dzuba, V. V. Flambaum, and A. Ong, Optical transitions in highly charged californium ions with high sensitivity to variation of the fine-structure constant, *Phys. Rev. Lett.* **109**, 070802 (2012).
- [45] K. Beloy, Trap-induced ac zeeman shift of the thorium-229 nuclear clock frequency, *Phys. Rev. Lett.* **130**, 103201 (2023).
- [46] T. Rosenband, D. Hume, P. Schmidt, C.-W. Chou, A. Brusch, L. Lorini, W. Oskay, R. E. Drullinger, T. M. Fortier, J. E. Stalnaker, *et al.*, Frequency ratio of al^+ and hg^+ single-ion optical clocks; metrology at the 17th decimal place, *Science* **319**, 1808 (2008).
- [47] S. M. Brewer, J.-S. Chen, A. M. Hankin, E. R. Clements, C. W. Chou, D. J. Wineland, D. B. Hume, and D. R. Leibbrandt, $^{27}\text{Al}^+$ quantum-logic clock with a systematic uncertainty below 10^{-18} , *Phys. Rev. Lett.* **123**, 033201 (2019).
- [48] E. Peik and C. Tamm, Nuclear laser spectroscopy of the 3.5 eV transition in Th-229, *Europhys. Lett.* **61**, 181 (2003).
- [49] P. O. Schmidt, T. Rosenband, C. Langer, W. M. Itano, J. C. Bergquist, and D. J. Wineland, Spectroscopy using quantum logic, *Science* **309**, 749 (2005).
- [50] J. C. Berengut, D. Budker, C. Delaunay, V. V. Flambaum, C. Frugiuéle, E. Fuchs, C. Grojean, R. Harnik,

R. Ozeri, G. Perez, and Y. Soreq, Probing new long-range interactions by isotope shift spectroscopy, *Phys. Rev. Lett.* **120**, 091801 (2018).

- [51] I. Counts, J. Hur, D. P. L. Aude Craik, H. Jeon, C. Leung, J. C. Berengut, A. Geddes, A. Kawasaki, W. Jhe, and V. Vuletić, Evidence for nonlinear isotope shift in Yb^+ search for new boson, *Phys. Rev. Lett.* **125**, 123002 (2020).
- [52] C. Solaro, S. Meyer, K. Fisher, J. C. Berengut, E. Fuchs, and M. Drewsen, Improved isotope-shift-based bounds on bosons beyond the standard model through measurements of the $^2\text{D}_{3/2} - ^2\text{D}_{5/2}$ interval in Ca^+ , *Phys. Rev. Lett.* **125**, 123003 (2020).
- [53] M. S. Safronova, D. Budker, D. DeMille, D. F. J. Kimball, A. Derevianko, and C. W. Clark, Search for new physics with atoms and molecules, *Rev. Mod. Phys.* **90**, 025008 (2018).
- [54] W. R. Johnson, *Atomic structure theory* (Springer, 2007).

End Matter

Analytical Methods – To obtain all the total angular momenta J for the ground-state configuration of each cell in the periodic table Fig. 1, we employ the jj coupling scheme based on the particle creation and annihilation operators. For two-electron systems, this is [54]

$$|JM\rangle = \sum_{m_a, m_b} C_{ab}^{JM} a_a^\dagger a_b^\dagger |0\rangle. \quad (3)$$

Here, $|JM\rangle$ is the energy eigenstate with a total angular momentum J and magnetic component M , and $|0\rangle$ the vacuum state. a_i^\dagger ($i = a, b$) creates one electron in the relativistic orbital with angular momentum j_i and magnetic component m_i . $C_{ab}^{JM} = C(j_a, j_b, J; m_a, m_b, M)$ with ($M = m_a + m_b$) is the corresponding Clebsch-Gordan coefficient that can be calculated via software such as Mathematica. As we are interested in the ground-state configurations, such as the np_+^2 , nd_-^2 , nd_+^2 , nf_-^2 , and nf_+^2 , one always has $j_a = j_b$. After accounting for the Pauli's exclusion principle, all allowed combinations of electron occupations can be determined, and are listed in the supplementary Tables S1-S4. With similar procedures, one can also obtain the CSFs for three and four electron systems, namely, the nd_+^3 , nf_-^3 , nf_+^3 , and nf_+^4 configurations.

In the following, we take the nd_+^2 and nf_-^2 configurations as an example to demonstrate the analytical considerations discussed in the main text. As shown in Table S2, there is only one occupation scheme for both $|M = 4\rangle$ and $|M = 3\rangle$ state. As these two Fock states will be accounted into the magnetic levels for the state with $J = 4$, it means that there is no state with $J = 3$ allowed in such a configuration. With similar considerations, one can also exclude the $J = 1$ state. Therefore, only the states with $J = 4, 2, 0$ are allowed in the nd_+^2 and nf_-^2 configurations. With the help of Eq. (3), the three $|M = 0\rangle$ Fock states can be used to construct the

corresponding three atomic states

$$\begin{aligned} |00\rangle &= \sqrt{\frac{1}{3}} S_{\frac{1}{2}, -\frac{1}{2}} - \sqrt{\frac{1}{3}} S_{\frac{3}{2}, -\frac{3}{2}} + \sqrt{\frac{1}{3}} S_{\frac{5}{2}, -\frac{5}{2}}, \\ |20\rangle &= -\sqrt{\frac{8}{21}} S_{\frac{1}{2}, -\frac{1}{2}} + \sqrt{\frac{1}{42}} S_{\frac{3}{2}, -\frac{3}{2}} + \sqrt{\frac{25}{42}} S_{\frac{5}{2}, -\frac{5}{2}}, \\ |40\rangle &= \sqrt{\frac{2}{7}} S_{\frac{1}{2}, -\frac{1}{2}} + \sqrt{\frac{9}{14}} S_{\frac{3}{2}, -\frac{3}{2}} + \sqrt{\frac{1}{14}} S_{\frac{5}{2}, -\frac{5}{2}}, \end{aligned}$$

with the Slater determinants being defined as

$$S_{ab} = \frac{1}{\sqrt{2}} (a_a^\dagger a_b^\dagger - a_b^\dagger a_a^\dagger) |0\rangle = \frac{1}{\sqrt{2}} (|ab\rangle - |ba\rangle).$$

With the above wavefunctions, one can proceed to calculate the energy of these atomic states. By defining the closed-shell core as the vacuum state, one has the energy

$$E_{JM} = 2\epsilon + \sum_{m_a m_b} \sum_{m_c m_d} C_{ab}^{JM} C_{cd}^{JM} g_{abcd},$$

with ϵ being the one-particle energy of the electron in the nd_+ or nf_- orbital, and $g_{abcd} = \langle ab | \frac{1}{r_{12}} | cd \rangle$ the 2-body matrix elements describing electron-electron Coulomb interactions. With further mathematical derivations, it can be proved that E_{JM} is independent of the magnetic component M such that

$$E_4 = 2\epsilon + R_0 - \frac{4}{35} R_2 - \frac{1}{63} R_4, \quad (4)$$

$$E_2 = 2\epsilon + R_0 + \frac{4}{175} R_2 - \frac{1}{21} R_4, \quad (5)$$

$$E_0 = 2\epsilon + R_0 + \frac{8}{35} R_2 + \frac{2}{21} R_4. \quad (6)$$

Here, $R_k = \int dr_1 \int dr_2 \rho(r_1) \rho(r_2) r_{<}^k / r_{>}^{k+1}$ [$k = 0, 2, 4$, and $r_{>} = \max(r_1, r_2)$ and $r_{<} = \min(r_1, r_2)$] is the Slater integral of rank k [18], and $\rho(r)$ the radial electron density of the nd_+ or nf_- orbital. As R_k is always positive and $R_2 > R_4$, it is obvious that $E_4 < E_2 < E_0$. The common term $2\epsilon + R_0$ in the energies of all three CSFs indicates that the excitation energies of the $J = 2, 0$ states are mainly determined by electron-electron interactions.

Numerical Methods — The level structures, lifetimes and line strengths mentioned in the main text were calculated via the *ab initio* fully relativistic multiconfiguration Dirac-Hartree-Fock (MCDHF) and relativistic configuration interaction (RCI) methods implemented in the GRASP2018 code [23]. Within this approach, the many-electron atomic state function (ASF) is constructed as a linear combination of configuration state functions (CSFs) with common total angular momentum (J), magnetic (M), and parity (P) quantum numbers:

$$|\Gamma P J M\rangle = \sum_k c_k |\gamma_k P J M\rangle.$$

Each CSF $|\gamma_k P J M\rangle$ is built from products of one-electron orbitals (Slater determinants), jj -coupled to the

appropriate angular symmetry and parity, and γ_k represents orbital occupations, together with orbital and intermediate quantum numbers necessary to uniquely define the CSF. Γ collectively denotes all the γ_k involved in the representation of the ASF. c_k is the corresponding mixing coefficient. The radial wave function for each orbital is obtained via solving the self-consistent MCDHF equations under the Dirac–Coulomb Hamiltonian. Then, the RCI method is applied to account for corrections arising from mass shift, quantum electrodynamic and Breit interactions.

As there are more than 700 HCI clock candidates, and to identify the positions of the reference ions listed in the periodic table Fig. 1, more than 1000 ions need to be calculated. Therefore, it is time consuming to fully account for the correlation effects for all these ions. Luckily, the correlation effects may shift the excitation energies, they do not modify the conclusions discussed in the main text. Therefore, only the correlation effects arising from single-electron excitations from the $\{n(l-1), nl\}$ valence orbitals to all the $\{n+1\}$ correlation orbitals are included in the GRASP2018 calculations.

ACKNOWLEDGMENTS

C.L thanks Dr. Li Han and Dr. Suvam Singh for discussions and reading the manuscript.

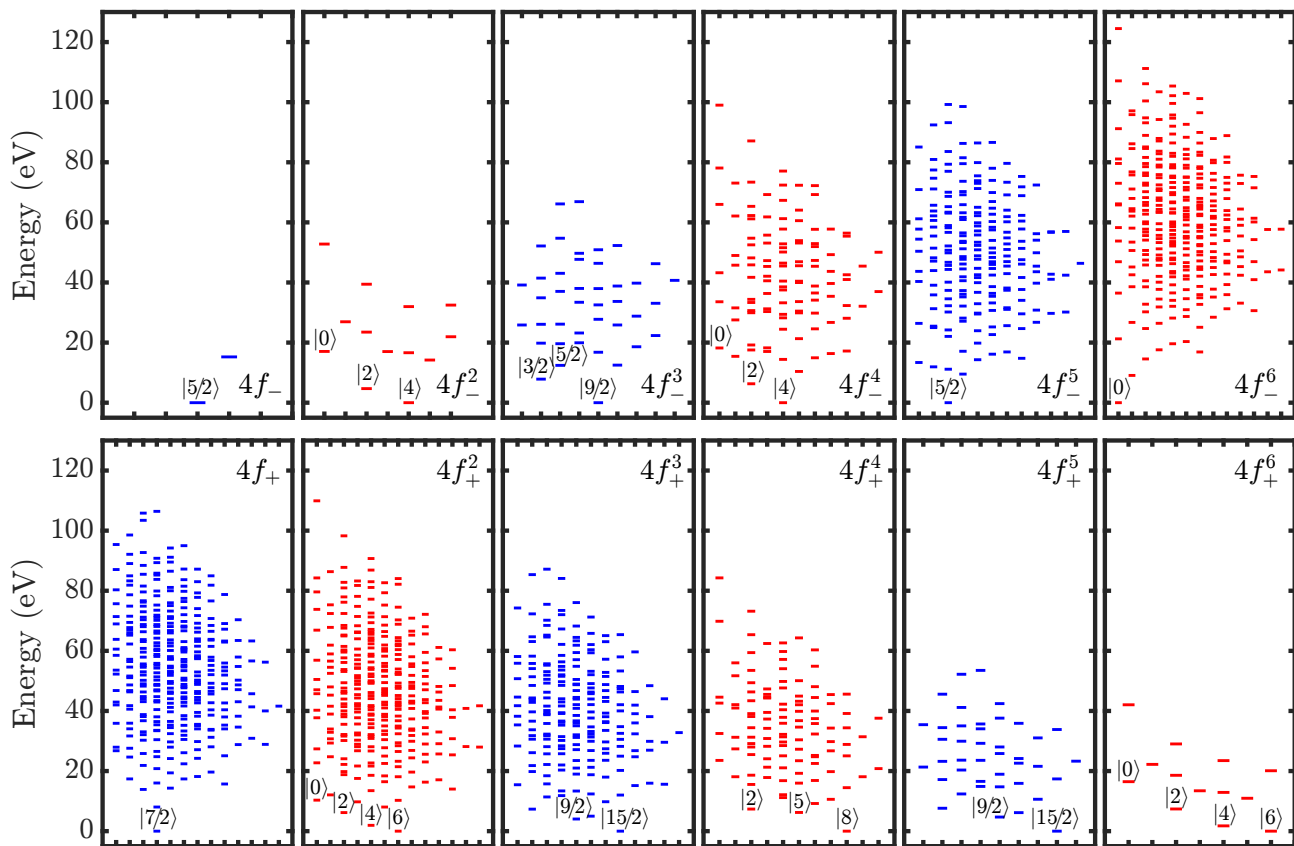


Figure S1. Level structure of highly charged uranium ions: the seventh row of the periodic table shown in Fig. 1.

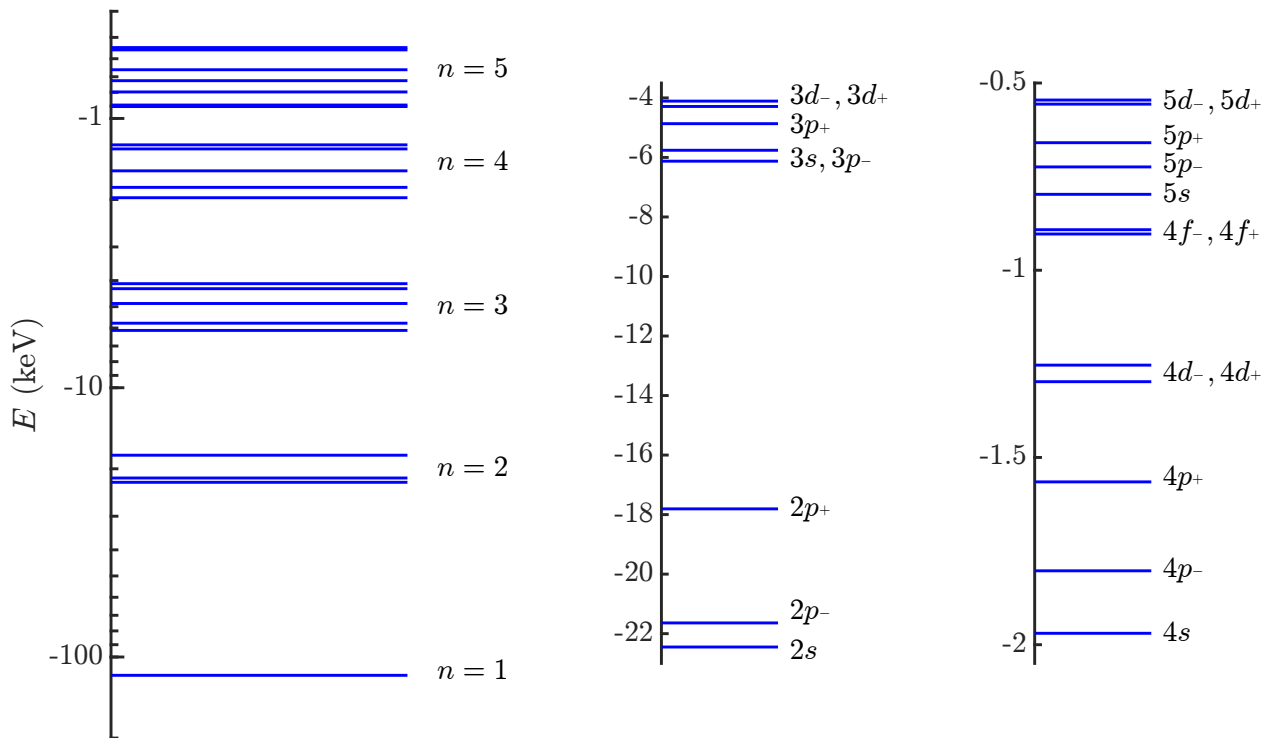


Figure S2. Energies of the relativistic orbitals in U^{22+} ($[Er]5d^2$). Results are obtained via DHF calculations.

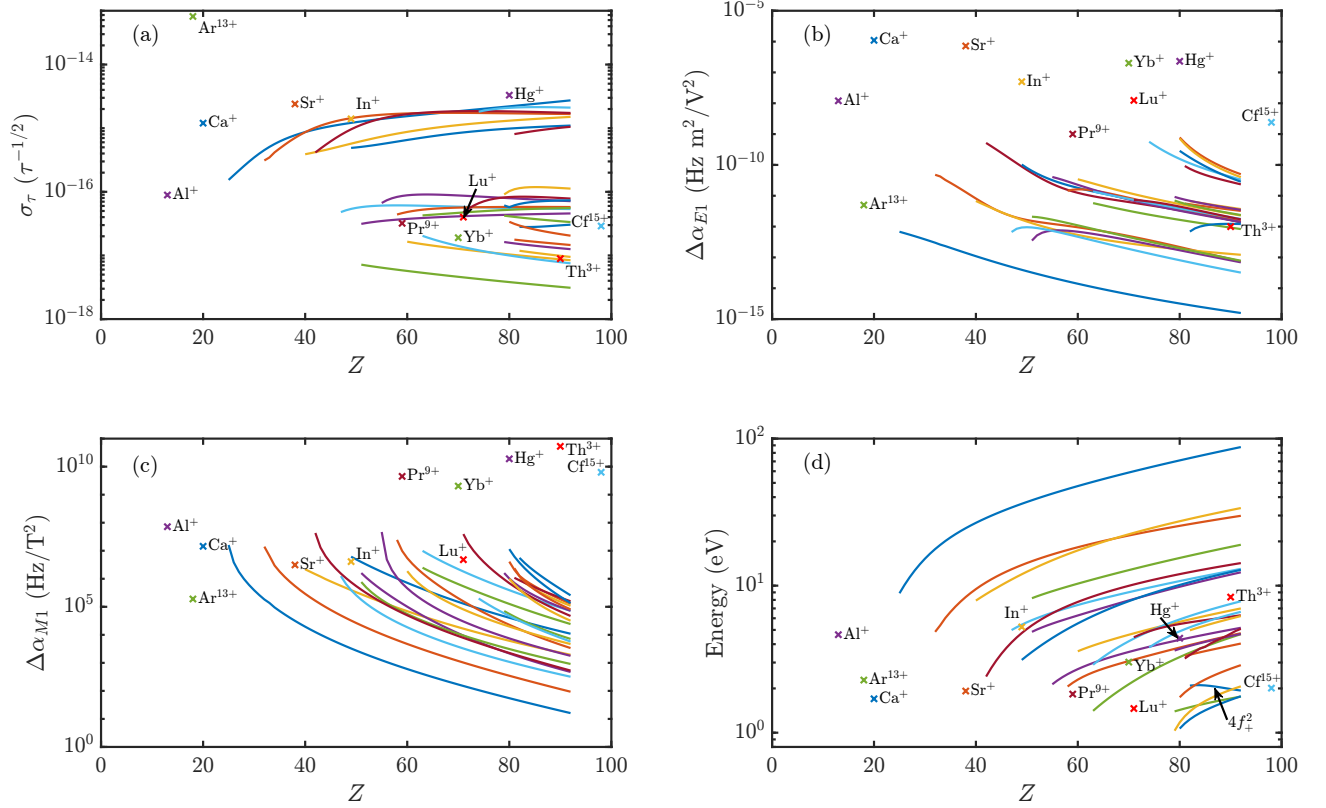


Figure S3. **Superior clock properties of the HCI clock candidates.** (a) the projected instability σ_τ , (b) the differential electric-dipole polarizability $\Delta\alpha_{E1}$, (c) differential magnetic-dipole polarizability $\Delta\alpha_{M1}$, and (d) transition energy of the HCI clock candidates are plotted as a function of the nuclear charge Z . With a total of more than 700 HCIs, each line in **a-c** corresponds to a relevant isoelectronic sequence denoted by the colored cells in the periodic table Fig. 1. For odd Z , we have neglected hyperfine interactions which is valid for their even isotopes with a zero nuclear spin. The details of their values can be found in the supplements. The corresponding values for singly charged ion clocks [12, 42], Ar^{13+} [11], Pr^{9+} [43], Cf^{15+} [44], and the nuclear clock $^{229}\text{Th}^{3+}$ [45] are presented for comparison. For the energies shown in (d), there is an exceptional line corresponding to the Xe-like isoelectronic sequence ($4f_+^2$). This line shows that the transition energy decreases for large Z . We found that it is due to a strong mixing between the states in the $4f_+^2$ configuration with the states in the $4f_-^{6-q}4f_+^{2+q}$ configurations. Here, q is the number of electrons being excited from the $4f_-$ orbital to the $4f_+$ orbital. When only the $4f_+^2$ configuration is considered, one would obtain the same increasing trend as observed in the other isoelectronic sequences.

Table S1. **Basis set for the Slater determinants of np_+^2 and nd_-^2 configurations.** In total, there are $C_4^2 = 6$ states that can be used to construct the $J = 2, 0$ CSFs.

$M_J \backslash m_j$	3/2	1/2	-1/2	-3/2
2	×	×		
1	×		×	
0	×			×
0		×	×	
-1		×		×
-2			×	×

Table S2. **Basis set for the Slater determinants of the nd_+^2 and nf_-^2 configurations.** In total, there are $C_6^2 = 15$ states that can be used to construct the $J = 4, 2, 0$ CSFs.

$M_J \backslash m_j$	5/2	3/2	1/2	-1/2	-3/2	-5/2
4	×	×				
3	×		×			
2	×			×		
1	×				×	
0	×					×
2		×	×			
1		×		×		
0		×			×	
-1		×				×
0			×	×		
-1			×		×	
-2			×			×
-2				×	×	
-3				×		×
-4					×	×

Table S3. **Basis set for the Slater determinants of the nd_+^3 and nf_-^3 configurations.** In total, there are $C_6^3 = 20$ states that can be used to construct the $J = 9/2, 3/2, 5/2$ CSFs.

$M_J \backslash m_j$	5/2	3/2	1/2	-1/2	-3/2	-5/2
9/2	×	×	×			
7/2	×	×		×		
5/2	×	×			×	
3/2	×	×				×
5/2	×		×	×		
3/2	×		×		×	
1/2	×		×			×
1/2	×			×	×	
-1/2	×			×		×
-3/2	×				×	×
3/2		×	×	×		
1/2		×	×		×	
-1/2		×	×			×
-1/2		×		×	×	
-3/2		×		×		×
-5/2		×			×	×
-3/2			×	×	×	
-5/2			×	×		×
-7/2			×		×	×
-9/2				×	×	×

